Approaches to structure and dynamics of biological systems by electron-paramagnetic-resonance spectroscopy
Scarpelli, F.

Appendix A

Anti-parallel aggregation of WALP peptides in DOPC

The study of WALP spin labeled at the central position had suggested linear aggregates in DOPC and cluster aggregates in DPPC, both at 120 K (Chapter 4). An anti-parallel arrangement of the peptides within the linear aggregates was proposed from theoretical [1] and experimental studies [2]. In order to investigate whether the line aggregates in DOPC contain the WALP peptides in a parallel or anti-parallel arrangement, a set of cw-EPR experiments was performed on WALP spin labeled at the N- or the C-terminal positions (SL-N-WALP and SL-C-WALP) at 120 K. In the present appendix, we describe a model that can be used to interpret the broadening of the EPR spectra due to anti-parallel aggregates.

Results

In the following, the dipolar interaction was calculated for models of anti-parallel aggregates. For a pair of pure SL-N (or C) WALP in an anti-parallel arrangement (Fig.1a), the dipolar interaction of two electron spins will cause a broadening

$$\left\langle \Delta\Delta B^2 \right\rangle = p\frac{1}{\left(L\right)^6} = p\frac{1}{\left(\sqrt{D^2+R^2}\right)^6} \tag{1}$$

Here L is the distance between the two spins, and D and R, defined in Fig. 1, are 3 nm and 1 nm respectively.
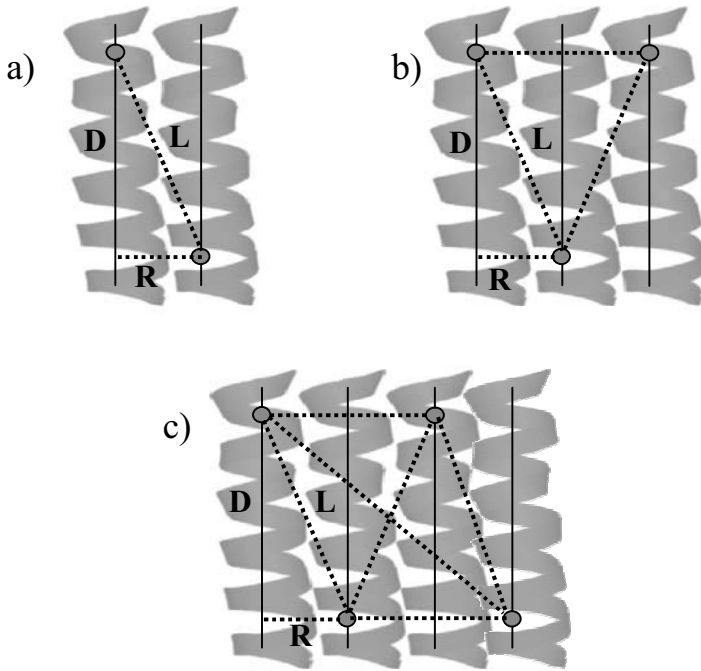
Fig. 1: Schematic representation of line aggregates with anti-parallel arrangements of the trans-membrane helices (WALP). The circle represents the spin label position. a) dimer; b) trimer; c) tetramer.

Assuming that the aggregates are modeled as having a fixed distance R between nearest neighbors, the $\langle \Delta\Delta B^2 \rangle$ value for a trimer and a tetramer anti-parallel aggregate, Fig.1 b and c, is

$$\left\langle \Delta\Delta B^2 \right\rangle_{Trimer} = p \bigg/ 3 \left[\frac{2}{(2R)^6} + \frac{4}{\left(\sqrt{D^2 + R^2} \right)^6} \right] \tag{2}$$

$$\left\langle \Delta\Delta B^2 \right\rangle_{Tetramer} = \frac{P}{4}\left[\frac{4}{(2R)^6} + \frac{6}{\left(\sqrt{D^2+R^2}\right)^6} + \frac{2}{\left(\sqrt{D^2+(3R)^2}\right)^6} \right] \qquad (3)$$

The largest aggregate for which calculations are performed concerns a tetramer because the data analysis in Chapter 4 suggests a tetramer as the most likely aggregate size.

The $\langle\Delta\Delta B^2\rangle$ values for a dimer, a trimer and a tetramer, calculated using this model, are shown in Table 1.

Table 1
Anti-parallel and parallel aggregate model: Calculated broadening of pure SL-N (or C) WALP

Aggregate type	Calculated Broadening Anti-parallel $<\Delta\Delta B^2>(T^2)$	Calculated Broadening Parallel $<\Delta\Delta B^2>(T^2)$
Dimer	$1.56*10^{-9}$	$1.56*10^{-6}$
Trimer	$1.83*10^{-8}$	$2.09*10^{-6}$
Tetramer	$2.68*10^{-8}$	$2.36*10^{-6}$

For a mixed sample (50% SL-N-WALP and 50% SL-C-WALP) the previous model has to be modified. For an anti-parallel arrangement of the peptides the chances that the spins will be at a distance R to each other (SL-C and SL-N WALP as the closest neighbor, Fig. 2a) or at a distance L (SL-N and SL-N WALP (or SL-C and SL-C) as closest neighbor, Fig. 2b) are equal. Therefore, a model that takes into account all the possible combinations and the weight that each of them has on the broadening, has been made.
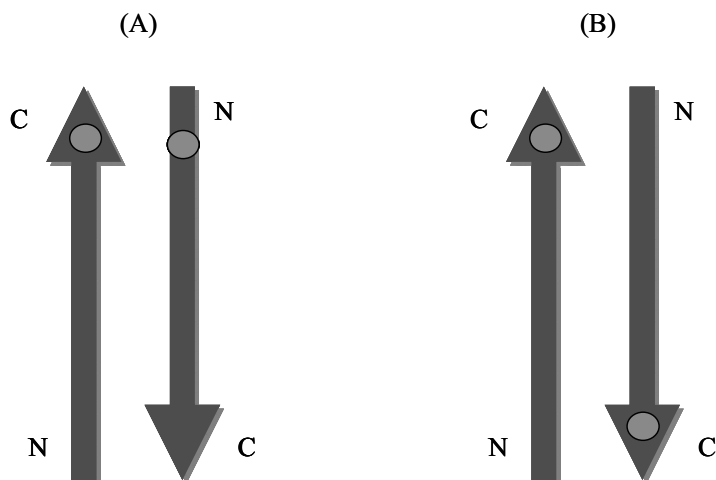
Fig. 2: Schematic representation of an anti-parallel dimer for mixed sample (50% SL-N-WALP and 50% SL-C-WALP). The circle represents the spin label position.(A) SL-C and SL-N as closest neighbor; (B) SL-C and SL-C as closest neighbour.

The calculated $<\Delta\Delta B^2>$ for the mixed SL-N and SL-C WALP are shown in Table 2.

Table 2

Calculated broadening of mixed SL-N and SL-C WALP, anti-parallel arrangement

Aggregate type	Calculated Broadening $<\Delta\Delta B^2>(T^2)$
Dimer	$7.08*10^{-7}$
Trimer	$1.05*10^{-6}$
Tetramer	$1.19*10^{-6}$

Discussion

The distance among spins for the pure SL-N (or C) WALP in the anti-parallel aggregate is bigger than the one in the parallel arrangement and this results in a smaller dipolar broadening, see Table 1.

The small calculated $<\Delta\Delta B^2>$ for the anti-parallel arrangement is in agreement with the experimental data (see result Chapter 4). Indeed the comparison of the pure SL-N and SL-C-WALP spectra with the diamagnetically diluted ones has shown such a small broadening value, $<\Delta\Delta B^2>$, that it can not be discriminated within the experimental uncertainty. If the aggregates were composed of WALP in a parallel arrangement we would have had a bigger $<\Delta\Delta B^2>$ value from the broadening of the spectra. This suggests that the arrangement of the peptides is most likely anti-parallel or random, and, from the result obtained by E. Sparr and coworkers we conclude that anti-parallel arrangement is the most probable [2,3].

To measure the broadening due to dipolar interaction for spins separated by a certain distance L (anti-parallel arrangement), the WALP has to be spin labeled positions other than the C- or N- terminus. For a pure SL-N (or C-) WALP, for which the spin labels are at a position that makes D = 0.6 nm the calculated broadening has a detectable value. In this case for a tetramer aggregate $<\Delta\Delta B^2>$ will be $1.0*10^{-6}$ T^2, and this dipolar broadening can be easily detected by EPR, see Fig. 6 in Chapter 4.

Reference List

1. Yano, Y.; Matsuzaki, K. *Biochemistry* **2006,** *45*, 3370-3378.

2. Sparr, E.; Ash, W. L.; Nazarov, P. V.; Rijkers, D. T. S.; Hemminga, M. A.; Tieleman, D. P.; Killian, J. A. *Journal of Biological Chemistry* **2005,** *280* (47), 39324-39331.

3. Sparr, E.; Ganchev, D. N.; Snel, M. M. E.; Ridder, A. N. J. A.; Kroon-Batenburg, L. M. J.; Chupin, V.; Rijkers, D. T. S.; Killian, J. A.; de Kruijff, B. *Biochemistry* **2005,** *44* (1), 2-10.

Appendix B

The longitudinal relaxation time (T_1) of Fe(III) in cytochrome *f*: power saturation

The applicability of the RIDME sequence (Chapter 5) depends on the longitudinal relaxation of the B spins. Here we show how the longitudinal relaxation time (T_1) of the Fe(III) center in the spin labeled cytochrome *f* protein mutant Q104C may be determined by the microwave power saturation method. In this method T_1 is measured from the effect of the microwave power on the intensity of the EPR line. For low microwave power, the rate of the induced transitions is small and the line intensity is proportional to that rate, which is given by the square root of the microwave power. For higher microwave powers such that the induced rate becomes comparable to the rate of T_1 relaxation, the line intensity increases less strongly than at low powers. At even higher microwave powers the line intensity becomes constant or even decreases.

The dependence of the line intensity on the power depends on whether the EPR signal is homogeneously or inhomogeneously broadened. The EPR signal of the Fe(III) center is inhomogeneously broadened, which means that we observe an envelop that consists of a distribution of individual resonant lines (Fig. 1). The shape of the envelop is Gaussian, while the individual lines have a Lorentzian line shape. The width of the whole Gaussian envelop is given by $\Delta\omega_G$. The width of the individual Lorentzian lines is given by [1]

$$\Delta\omega_L = \frac{1}{T_2} \quad ,$$

(1)

where T_2 is the transversal relaxation time.

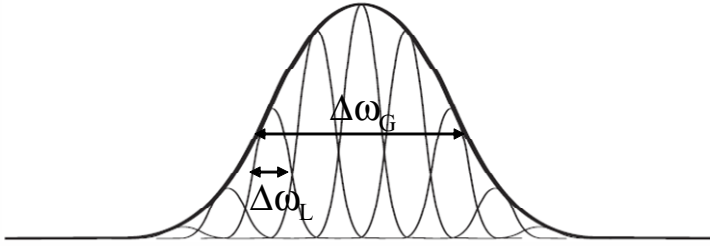The procedure to obtain T_1 from the power dependence is described below.

Fig. 1: Superposition of Lorentzian lines (thin lines) constituting an inhomogeneously broadened Gaussian line (thick line). The width of the envelop is indicated by the Gaussian width $\Delta\omega_G$. The width of the individual lines, which constitute the envelop, is indicated by the Lorentzian width $\Delta\omega_L$.

Experimental methods

The X-band cw EPR measurements have been performed using an ELEXSYS E 680 spectrometer (Bruker, Rheinstetten, GE) equipped with a helium gas-flow cryostat and a rectangular cavity. The EPR spectra were recorded at 7 K using a modulation amplitude of 1.5 mT. The intensity of the low-field EPR line was measured at different power levels in a range from 0.052 mW to 200 mW. The EPR spectra were baseline corrected using Xepr software (Bruker Biospin, Rheinstetten, Germany). Because of the baseline correction, the estimation of T_1 has an error of 20%. The fit was done using MatLab (MathWorks, MA, USA).

The amplitude of the microwave magnetic field (H_1) and the incident microwave power (P) are related by [1,2]

$$H_1 = g^I \sqrt{QP} \quad , \tag{2}$$

where g^I depends on the geometry of the cavity, Q is the quality factor of

the cavity. For the rectangular cavity used in our measurements $g^I =$ 0.0028 $mT / \sqrt{mW}$ [3] and Q = 4000.
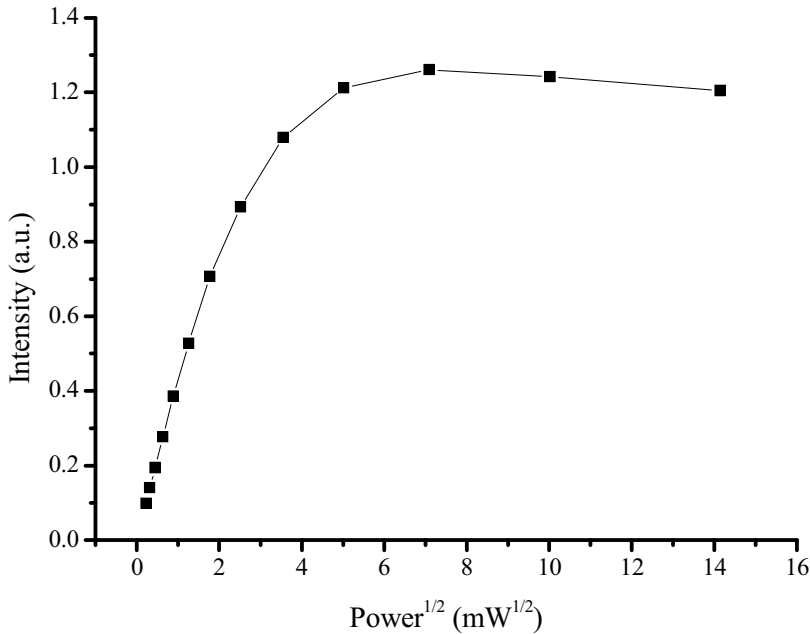

Fig. 2: The intensity of the low field EPR signal of Fe(III) as a function of the square root of the microwave power.

Results

In Fig. 2 a plot of the intensity of the low-field component of the EPR signal of the Fe(III) (Fig. 3) as a function of the square root of the microwave power is shown. The intensity of the EPR line became almost constant for high values of the microwave power [4], between 50 mW and 200 mW, and the shape of the line can be fitted by a Gaussian function (Fig. 3b). These observations confirm the inhomogeneous broadening of the Fe(III) signal.

The longitudinal relaxation rate is related to the *saturation factor* [3] Z. The Z value is given by

$$Z = \frac{1}{1 + H_1^2 \gamma^2 T_1 T_2} \quad ,$$

(3)

where γ is the magnetogyric ratio ($\gamma = 2.8 * 10^{10}$ s^{-1} T^{-1}).
From the power P the value of H_1 can be calculated according to Eq. 2.
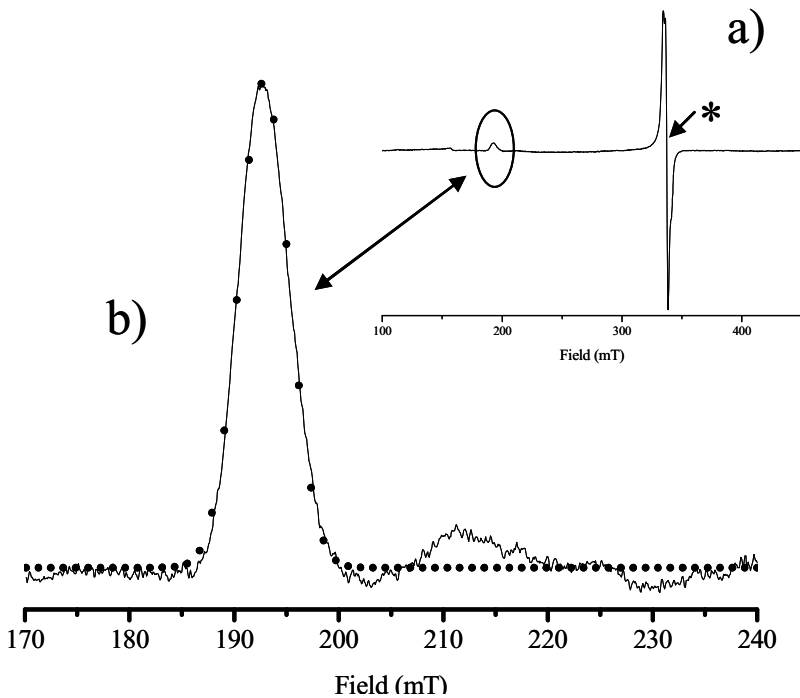

Fig. 3: a) The EPR spectrum of the spin-labeled cytochrome f mutant Q104C, recorded with a microwave power of 3.14 mW. The intense signal indicated by the asterisk is due to the nitroxide spin label. b) The low field line of the EPR signal shown in a), and the fit of this line to a Gaussian (black dots). The EPR spectrum has been baseline corrected.

For $H_1 = H_{1/2}$, corresponding to a value of $P = P_{1/2}$ such that the saturation factor Z becomes 0.5, we obtain

$$H_{1/2}^2 \gamma^2 T_1 T_2 = 1 \quad ,$$

(4)

and consequently

$$T_1 = \frac{1}{H_{1/2}^2 \gamma^2 T_2} \quad .$$

(5)

To obtain $H_{1/2}$ we need $P_{1/2}$. Knowing $H_{1/2}$, only T_2 is needed to obtain T_1 from Eq. 5.

The $P_{1/2}$ value can be obtained by fitting the normalized intensity Y_n of the EPR signal with the following equation [3]

$$Y_n = \frac{Y/\sqrt{P}}{Y_0/\sqrt{P_0}} = \frac{1}{\left[1+\left(P/P_{1/2}\right)\right]^{b/2}} ,$$

(6)

where Y_n is the normalized line intensity, Y is the line intensity obtained at the power P, and Y_0 is the line intensity obtained at a power P_0 of 0.399 mW, under nonsaturating conditions. Fitting this equation to the data points results in the plot shown in Fig. 4. The fit yields the parameters $P_{1/2}$ and b, where b is called the inhomogeneity parameter [3], which can be expressed as

$$\log b = \frac{\Delta\omega_L}{\Delta\omega_G}$$

(7)

where $\Delta\omega_G$ is measured from the experimental spectrum. In our case, the low-field EPR line has a $\Delta\omega_G$ of 6 mT. From the fit we have obtained the parameters: $b = 1.048$ and $P_{1/2} = 9$ mW. As mentioned previously, $\Delta\omega_L$ is related to T_2. Therefore, knowing b and $\Delta\omega_G$, the $\Delta\omega_L$ value has been calculated from Eq. 7, which results in $T_2 = 45$ ns. Having calculated $H_{1/2}$ and knowing T_2, a value of 102 μs is obtained for T_1.

In Chapter 5, from the modulation depth of the RIDME trace, we have detected two components of T_1 (148 μs and 13 μs) and attributed this to the anisotropy of this relaxation time. In the present study, we were able to determine T_1 from the effect of the microwave power on the signal corresponding to one of the canonic orientations of the Fe(III) center. To measure the full extend of the anisotropy, a larger number of orientations would have to be measured. Given the spread of the EPR signal of Fe(III) over 300 mT, at many of these spectral positions the signal intensity is probably too small to do so. This precluded us to detect any orientation dependence of T_1. The T_1 value of 102 μs is closer to the larger T_1 component obtained from the RIDME traces.
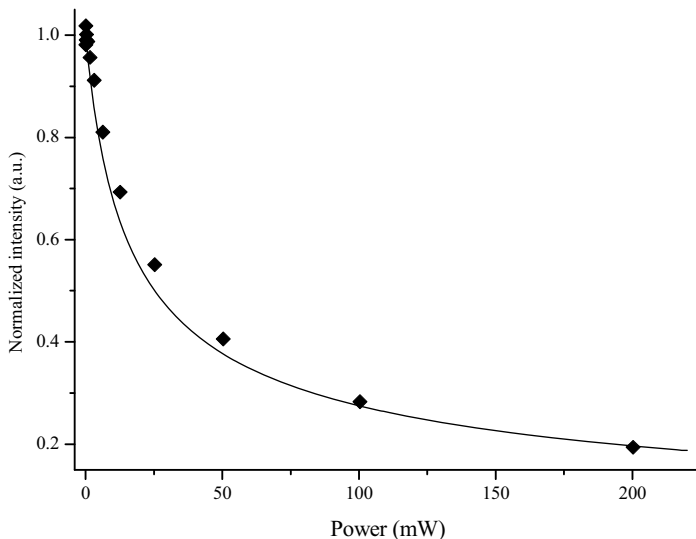

Fig. 4: The plot of the normalized line intensity Y_n (see text) of the low-field EPR signal of Fe(III) as a function of the microwave power. The black diamonds represent the data points. The black curve is the fit.

Reference List

1. Castner, T. G. *Physical Review* **1959,** *115* (6), 1506-1515.
2. Poole, C. P. J. *Electron Spin Resonance: A Comprehensive Treatise on Experimental Techniques;* Dover Publications: Mineola, New York, 1996.
3. Sahlin, M.; Graslund, A.; Ehrenberg, A. *Journal of Magnetic Resonance* **1986,** *67* (1), 135-137.
4. Portis, A. M. *Physical Review* **1953,** *91* (5), 1071-1078.